

1 **Technical Note: Testing an improved index for analysing storm discharge-concentration hysteresis.**

2 Lloyd, C.E.M.^{1,2}, Freer, J.E.², Johnes, P.J.² and Collins, A.L.³

3 ¹ School of Chemistry, University of Bristol, Cantock's Close, Bristol, BS8 1TS, UK.

4 ² School of Geographical Sciences, University of Bristol, University Road, Bristol, BS8 1SS, UK.

5 ³Department of Sustainable Soils and Grassland Systems, Rothamsted Research, North Wyke,
6 Okehampton, EX20 2SB, UK

7 * Corresponding author: Charlotte Lloyd

8 Address: School of Chemistry, University of Bristol, Cantock's Close, Bristol, BS8 1TS, UK.

9 e-mail: charlotte.lloyd@bristol.ac.uk

10 Telephone: +44 (0)117 3316795 Fax: +44 (0)117 927 7985

11

12 *Abstract*

13 Analysis of hydrochemical behaviour during storm events can provide new insights into the process
14 controls on nutrient transport in catchments. The examination of storm behaviours using hysteresis
15 analysis has increased in recent years, partly due to the increased availability of high temporal
16 resolution datasets for discharge and nutrient parameters. A number of these analyses involve the
17 use of an index to describe the characteristics of a hysteresis loop in order to compare different
18 storm behaviours both within and between catchments. This technical note reviews the methods for
19 calculation of the hysteresis index (HI) and explores a new more effective methodology. Each
20 method is systematically tested and the impact of the chosen calculation on the results is examined.
21 Recommendations are made regarding the most effective method of calculating a HI which can be
22 used for comparing data between storms and between different parameters and catchments.

23

24 *1. Introduction*

25 The analysis of hysteresis patterns is a key tool for the interrogation of in-stream physical and
26 chemical responses to storm events, which have been shown to be important periods for the
27 transport of nutrients and sediment within catchments (Bowes et al., 2003;Jarvie et al., 2002;Jordan
28 et al., 2007;Burt et al., 2015;Evans and Johnes, 2004). In the context of this paper, hysteresis is
29 defined as the nonlinear relationship between discharge and concentration of nutrients or sediment.
30 When discharge-concentration data are plotted a cyclic pattern is often observed, the strength of
31 the relationship is dependent on the nature of the lag in response between the two variables.
32 Quantification of hysteresis allows multiple storm behaviours to be examined between and within
33 catchments, for a wide range of hydrological and hydrochemical parameters. This can provide insight
34 into catchment function, allowing the development and testing of process-based understanding.
35 This type of analysis has been used in recent years by many authors investigating nutrient
36 concentration-discharge relationships in catchments of differing environmental character (e.g.
37 Bowes et al., 2015;Darwiche-Criado et al., 2015;Cerro et al., 2014;Rodriguez-Blanco et al.,
38 2013;Oeurng et al., 2010;Eder et al., 2010;Evans and Johnes, 2004) but, traditionally, has been used
39 for the examination of turbidity or suspended sediment data (e.g. Ziegler et al., 2014;House and
40 Warwick, 1998;Williams, 1989;Tena et al., 2014;Klein, 1984;Whiting et al., 1999). Hysteresis analysis
41 has been used to support the investigation of the temporal variations in nutrient transport to
42 streams as a means of characterising the likely contributing source areas and flow pathways linking
43 source to stream in complex landscapes (Outram et al., 2014;Bowes et al., 2015;Lloyd et al., 2016).
44 Similar hysteresis patterns can be observed for a variety of different reasons, however it is generally
45 assumed that clockwise hysteresis, caused by a small or no lag between discharge and concentration
46 suggests a source close to the monitoring point. Conversely, anti-clockwise hysteresis generally
47 signifies a longer lag between the discharge and concentration peak, suggesting that the source was
48 located further from the monitoring point. (Williams, 1989) provides a detailed summary of different
49 shape hysteresis plot and the possible mechanisms.

50 For hysteresis analysis to be effective and easy to interpret there is a need to develop an effective
51 method of classifying storms according to their hysteretic behaviour. Many papers have classified
52 storms into clockwise or anticlockwise responses, and described the strength of the hysteresis as
53 small or large (Bowes et al., 2015;Evans and Davies, 1998;Butturini et al., 2008). Other authors have
54 used an index approach, which allows a dimensionless quantification of the hysteresis, and thus,
55 comparison of hysteresis indices between catchments of differing size, morphology and hydrological
56 function. An index approach is also useful as it provides information about both the direction and
57 strength of the hysteresis. Hysteretic indices proposed by Butturini et al. (2008) provide semi-

58 quantitative methods to describe whether the measured parameter is enriched or diluted during a
59 storm event and to assess the area inside the hysteresis loop, along with its direction. Langlois et al.
60 (2005) propose a quantitative method which involves splitting the discharge hydrograph into the
61 rising and falling limb and fitting regression lines to each dataset. The hysteresis index is calculated
62 as the ratio (rising:falling) of the areas under the regression curves. Whilst this index provides a
63 quantitative solution, the authors suggest that the method should only be applied to simple uni-
64 directional loops, i.e. not those which exhibit figure-of-eight or more complex behaviours. A
65 quantitative index was also proposed by Lawler et al. (2006), which uses the ratio of the turbidity (or
66 other parameter) concentration on the rising and falling limb, at the mid-point in the discharge. The
67 mid-point in discharge is defined as 50% of the range in discharge during the storm event. This index
68 has been used by a number of other authors (McDonald and Lamoureux, 2009; Outram et al., 2014),
69 as it is flexible and can be applied to hysteresis loops of all shapes. However it is not without
70 limitations. In a recent paper, Aich et al. (2014) highlight that the index of Lawler et al. (2006) in its
71 current form becomes skewed at higher concentrations, with a smaller index calculated for loops of
72 the same shape and area in the case of storms commencing at a higher concentration (Figure 1a). In
73 addition, the calculation of the index using only the mid-point (50%) in discharge can be problematic.
74 Lawler et al. (2006) state that the mid-point was used as it avoids the often noisy sections at the
75 beginning and end of the loops. However, the result of the calculated index may be misleading in
76 many figure-of-eight scenarios, especially those which cross close to the mid-point in discharge (see
77 Figure 1b). The example shown in Figure 1b illustrates that a hysteresis index (HI) calculated at the
78 mid-point in discharge would suggest that there was very little hysteresis, even though there is a
79 strong effect but in different directions during different periods of the storm event. As suggested by
80 Lawler et al. (2006), the HI can be calculated at multiple increments through the flow range and an
81 average HI value gained. Against the above background, this technical note reports the impact of the
82 chosen method on the index values generated from a series of storms of varying size and hysteretic
83 shapes, using an adapted version of the Lawler et al. (2006) index (HI_{LA}). The paper also introduces a
84 new method for calculating the hysteresis index (HI_{new}) and, as a result of this analysis, suggests a
85 recommendation for the most appropriate calculation for a HI for storm-driven nutrient transport in
86 catchments.

87 *2. Methodology*

88 *2.1 Datasets*

89 The example uses a series of storms extracted from high-temporal resolution (15-min) data collected
90 on the River Wylfe at Brixton Deverill (Wiltshire, UK) as part of the Defra Demonstration Test

91 Catchment project (McGonigle et al., 2014) from March 2012 to March 2014. Detailed descriptions
92 of the field site and the datasets are available in previously published work (Lloyd et al., 2015, in
93 revision). For the purposes of this study, discharge data were obtained from the Environment
94 Agency gauge (Gauge Number 43806) and turbidity data were collected using a YSI 6-series sonde,
95 which was cleaned and calibrated once a month over the monitoring period. Turbidity (measured in
96 Nephelometric Turbidity Units (NTU)) was chosen for this study as it is the most widely examined
97 parameter in terms of hysteresis and the storms selected from the data set exhibit a wide range of
98 turbidity values and hysteretic shapes. A total of 66 storms were extracted for this analysis from the
99 two year observational data. A storm was classified as an increase in discharge of more than 20%
100 above baseflow and the end of the storm was determined by either a return to baseflow conditions
101 or when discharge began to rise again if another storm occurred before the system had returned to
102 baseflow conditions. Previous work had quantified the uncertainty associated with the discharge and
103 turbidity measurements (Lloyd et al., 2015; Lloyd et al., 2016) and this provided 100 resampled
104 iterations of each measured parameter for every storm, accounting for observational uncertainties,
105 for this analysis. Figure 2a-f(l) shows some example storms, where the boxes represent the 5th- 95th
106 percentile uncertainty range for each data point.

107 2.2 Lawler et al. (2006) method and modification

108 The HI was then calculated according to the standard method of Lawler et al. (2006) (HI_L) for
109 combinations of all 100 iterations of each of the storms to provide a distribution of HI when the mid-
110 point in discharge was calculated (50%). The Lawler et al. (2006) method was also adapted (HI_{LA}),
111 where HI was calculated at every 25%, 10%, 5% and 1% increments of the discharge (see Figure 3 for
112 visualisation) as shown below:

113 if $T_{RL} > T_{FL}$ (clockwise hysteresis):

$$114 \quad HI_L = \left(\frac{T_{RL}}{T_{FL}} \right) - 1 \quad (1)$$

115 Or, if $T_{RL} < T_{FL}$ (anti-clockwise hysteresis):

$$116 \quad HI_L = \left(-1 / \frac{T_{RL}}{T_{FL}} \right) + 1 \quad (2)$$

117

118 Where: T_{RL} is the value of turbidity at a given point in flow on the rising limb and T_{FL} is the value on
119 the falling limb.

120 When multiple sections per storm were calculated, the average value was taken to represent the HI
121 of the complete storm event. In some cases there were not corresponding values on both the falling
122 and rising limbs, when this occurs the maximum number of available pairs of data were used to
123 calculate the index. This only usually occurred at lowest discharges and when a large number of
124 intervals were being analysed. This meant that the number of missing pairs was small compared with
125 the available pairs (<5%) and as a result had little impact on the overall calculation. The analyses
126 were completed for both the raw data and for normalised storms to assess the impact of the
127 different analysis methods on the HI values obtained. The data were normalised using the following
128 equations:

$$129 \quad \text{Normalised } Q_i = \frac{Q_i - Q_{min}}{Q_{max} - Q_{min}} \quad (3)$$

$$130 \quad \text{Normalised } T_i = \frac{T_i - T_{min}}{T_{max} - T_{min}} \quad (4)$$

131 Where: Q_i/T_i is the discharge/turbidity at timestep i , Q_{min}/T_{min} is the minimum storm parameter value
132 and Q_{max}/T_{max} is the maximum storm parameter value.

133 2.3 Proposed new Hysteresis Index method (HI_{new})

134 A new method of calculating a HI was also tested (HI_{new}) with the aim of eliminating the impact of a
135 changing baseline value on the ratio as multiple measurements are taken from the same storm. The
136 new index uses the difference between the turbidity values on the rising and falling limbs of the
137 normalised storms, rather than a ratio, and effectively normalises the rising limb at every
138 measurement point, thereby resulting in an index between -1 and 1.

$$139 \quad HI_{new} = T_{RL_{norm}} - T_{FL_{norm}} \quad (5)$$

140 As with the other methods, the analysis was carried out using different intervals of discharge (25%,
141 10%, 5% and 1%) and the mean was used as the final HI value for the storm. The impact of this
142 number of chosen intervals of discharge on the magnitude of the resulting HI was tested.

143 The resulting distributions of HI values for each method were then scrutinised using boxplots.
144 Differences between the distributions of data for each storm were analysed statistically using
145 ANOVA where normality and variance assumptions were met, and the non-parametric alternative
146 Kruskal-Wallis-H on ranked data where the ANOVA assumptions did not hold. When a significant
147 difference between the groups was detected, a pairwise Tukey test was used to establish which of
148 the groups were contributing to the effect. The main aim of the analysis was to determine the point
149 at which sufficient intervals of discharge were used so that there was no statistically significant
150 difference between the different datasets for each storm.

151 *3. Results and discussion*

152 A total of 66 storms were analysed using the three methods for calculating the HI, which included 35
153 anti-clockwise loops, 11 clockwise loops, 12 figure-of-eight loops which were mainly anti-clockwise
154 and, 8 figure-of-eight loops which were mainly clockwise (loop shapes were examined by visual
155 inspection). The peak turbidity during the storms ranged between 10 and 392 NTU (mean = 91 NTU)
156 and the starting values were between 2 and 31 NTU (mean = 8 NTU). Figure 2 shows six example
157 storms (a-f, panel I) from the range of behaviour identified above, each with varying shape and size.
158 Table 1 summarises the number (and percentage) of storms tested which can be adequately
159 represented by the different discharge interval frequencies tested.

160 Figure 2a-f(II) shows the distributions of HI values (using HI_L) measured at only 50% of discharge are
161 often very different from the analyses which measure multiple sections across the loop (HI_{LA}). The
162 more complex the shape of the loop, the more measured sections are needed to represent it
163 adequately. The analysis shows that by using 5% increments of discharge (19 sections), 98% of the
164 storms analysed showed stable distributions and therefore no significant changes were observed
165 when additional increments were included. While including more increments of the loop in the
166 analysis does improve the HI results, it does not solve all of the issues highlighted earlier. Both HI_L
167 and HI_{LA} are sensitive to the size of the storm and, as a result, for a similar pattern in hysteresis but a
168 larger magnitude of storm, a comparatively smaller value would be calculated for the index, as
169 shown in Figure 1a. This means that the results generated for a series of storms are very difficult to
170 interpret and it is difficult to compare between individual storms and catchments. By normalising
171 the storms as described above and continuing to use the HI_{LA} method, the comparability of the
172 outputs between storms is improved as they are all assessed on the same scale. However, if multiple
173 increments of discharge are included, which has been shown to be beneficial, then effectively each
174 of the individual measured sections of the storm need to be normalised, otherwise the problem is
175 reduced but not eradicated. This problem is illustrated in Figure 1c, which shows an example of an
176 idealised and normalised storm where the width of the loop remains constant through most of the
177 storm. However at different quantiles of flow, HI value varies due to the loop gradient, the HI is
178 inflated towards the lower and reduced at higher quantiles of discharge. The HI_{new} was designed to
179 overcome this problem. The new index uses the range of turbidity values between the rising and
180 falling limb at each increment of discharge rather than the ratio, thereby directly quantifying the
181 width of the loop.

182 Figure 4 shows how the new index effectively normalises the rising limb and examines the relative
183 behaviour of the falling limb, thereby identifying the proportion of the storm occurring in a clockwise

184 or anti-clockwise phase. For this new method to be robust, it is necessary to normalise the data as
185 described earlier before the analysis. Figure 2a-f(III) show the example storms in their normalised
186 forms. The new index produces a value between -1 and 1, where 0 represents no hysteretic pattern
187 and positive values clockwise and negative values, anti-clockwise hysteresis. A figure-of-eight storm
188 will be represented as a weighted average of the intervals of discharge measured when the storm
189 was in a clockwise phase and when it was in an anticlockwise phase. Therefore, for example, if the
190 storm exhibits anti-clockwise behaviour for a large proportion of the storm event the average HI_{new}
191 will produce a negative number. It should be noted that in the unusual case that an exactly
192 symmetrical figure-of-eight storm is presented the index would produce a value of 0, suggesting no
193 hysteresis. Using the HI value in conjunction with loop area will however provide clarification as a
194 storm which has an HI of 0 but a positive loop area has to be a complex loop shape. The advantage
195 with our new technique is that the user can choose to interrogate other output metrics within these
196 results, such as the quantified loop area and the distribution of HI values calculated for each section
197 of the loop in addition to the averaged HI value. By looking at the distribution of values it is simple to
198 identify complex loop shapes such as figure-of-eight (due to both positive and negative values
199 calculated for the various loop sections) and ensures correct interpretation of the HI values.
200 Although we do not explore the advantage of these further analyses here, we suggest they
201 potentially provide a richer analyses of hysteresis dynamics that we aim to explore in future papers.

202 We suggest the new index provides a consistent approach to the core loop characteristics and
203 therefore is more easily interpretable by the user when comparing behaviour between storms or
204 field sites. Figure 2a-f(IV) show the resulting distributions of HI_{new} generated using varying
205 increments of discharge. The analysis shows that the distribution of calculated values was generally
206 more stable compared with the HI_{LA} method and, in many cases, fewer increments of discharge were
207 necessary to produce a statistically stable representation of the storm loop shape (Table 1). The
208 results demonstrate that increasing the increments to every 10% of discharge allowed 95% of storms
209 and using 5% increments allows 100% of storms to be robustly characterised in terms of their loop
210 shape, meaning that the addition of more sections did not significantly alter the distribution of HI
211 results.

212 *4. Conclusions and recommendations*

213 The concept of using an index to aid the quantification of storm hysteresis has been established for
214 over two decades. However few papers have chosen to use them, perhaps due to the limitations
215 associated with the most common methods. This technical note was designed to test systematically,
216 for the first time, the way that the HI is calculated and to quantify the impact of the chosen method

217 on the results. The analysis has led to a number of recommendations concerning how the HI should
218 be calculated in order to produce results which are both statistically robust and comparable
219 between storms and field sites. This technique is useful when the user's interest is in the relative
220 characteristics of the loop geometries. These recommendations are:

- 221 1. Storms should be normalised before analysis so that multiple storms can be robustly
222 compared.
- 223 2. A range method, such as the new index (HI_{new}) proposed here, should be used in preference
224 to a ratio method as it produces results which are easier to interpret, allowing quantification
225 of the extent of the hysteresis effect that can be directly compared between contrasting
226 catchments even when the magnitude of the storms varies greatly.
- 227 3. Multiple sections of each loop should be analysed so that the extent and direction of the
228 hysteresis can be accounted for throughout the flow range. Sections should be measured at
229 least every 10% of the discharge range, although every 5% is recommended as it is likely,
230 based on our analysis, to produce robust results for almost all storm sizes and shapes.
- 231 4. Examine the distribution of HI values calculated across the sections in addition to the
232 averaged value, as this aids robust classification of complex loop shapes, including figure-of-
233 eight loops.

234 Undertaking the analysis of hysteresis loops using these guidelines improves the clarity of the
235 hysteresis index as a diagnostic tool for the analysis of storms and how discharge-concentration
236 patterns vary. The new index (HI_{new}) is able to describe robustly the shape and direction of a
237 hysteretic pattern in storms of any size, and can be used to compare storms from multiple
238 catchments. This means that the index becomes more useful as it has the potential to become a
239 standardised analytical technique that can be utilised by the water quality research community.
240 Lloyd et al. (2016) illustrates the use of the new hysteresis index to investigate storm behaviours
241 across different nutrient parameters and between contrasting catchments. This study exemplifies
242 the power of having such a summary statistic, as different parameters and field sites can be rapidly
243 and robustly compared. The information provided by the HI_{new} can be used in conjunction with other
244 common metrics such as storm maximum concentration to produce a useful and robust quantitative
245 representation of storm hydrochemical behaviour. Standardising approaches for the calculation of
246 HI would provide a useful tool for assessing storm behaviour. This is timely given the marked
247 increase in the number of catchment scale water quality monitoring initiatives, which are now
248 employing high temporal resolution monitoring to improve understanding of pollution sources and
249 delivery pathways. Our ongoing research is exploring the use of this new index in understanding
250 changing catchment dynamics associated with storm behaviours.

251 *Acknowledgements*

252 The authors gratefully acknowledge the funding provided by Defra project WQ0211 (the Hampshire
253 Avon Demonstration Test Catchment project) and NERC Grant NE/1002200/1 (The Environmental
254 Virtual Observatory Pilot), and the access to the Brixton Deverill gauging site and flow data provided
255 by Geoff Hardwicke at the Environment Agency.

256

257 Table 1: showing the increments of discharge measured and the corresponding number of storms
258 (out of 66 analysed) and the percentage of storms which can be robustly* characterised using
259 different HI methods. *Where adding extra measurement sections does not statistically change the
260 distribution of HI vales for a storm.

Percentile increments	Sections measured	Storms (HI_L/HI_{LA})	Storms (HI_{new})
50%	1	5 (8%)	1 (1.5%)
25%	3	34 (52%)	41 (62%)
10%	9	55 (83%)	63 (95%)
5%	19	65 (98%)	66 (100%)
1%	99	66 (100%)	66 (100%)

261

262

263 5. References

264

265 Aich, V., Zimmermann, A., and Elsenbeer, H.: Quantification and interpretation of suspended-
266 sediment discharge hysteresis patterns: How much data do we need?, *Catena*, 122, 120-129,
267 10.1016/j.catena.2014.06.020, 2014.

268 Bowes, M. J., House, W. A., and Hodgkinson, R. A.: Phosphorus dynamics along a river continuum,
269 *Science of the Total Environment*, 313, 199-212, 10.1016/s0048-9697(03)00260-2, 2003.

270 Bowes, M. J., Jarvie, H. P., Halliday, S. J., Skeffington, R. A., Wade, A. J., Loewenthal, M., Gozzard, E.,
271 Newman, J. R., and Palmer-Felgate, E. J.: Characterising phosphorus and nitrate inputs to a rural river
272 using high-frequency concentration-flow relationships, *The Science of the total environment*, 511,
273 608-620, 10.1016/j.scitotenv.2014.12.086, 2015.

274 Burt, T. P., Worrall, F., Howden, N. J. K., and Anderson, M. G.: Shifts in discharge-concentration
275 relationships as a small catchment recover from severe drought, *Hydrological Processes*, 29, 498-
276 507, 10.1002/hyp.10169, 2015.

277 Butturini, A., Alvarez, M., Bernal, S., Vazquez, E., and Sabater, F.: Diversity and temporal sequences
278 of forms of DOC and NO₃-discharge responses in an intermittent stream: Predictable or random
279 succession?, *J. Geophys. Res.-Biogeosci.*, 113, 10.1029/2008jg000721, 2008.

280 Cerro, I., Sanchez-Perez, J. M., Ruiz-Romera, E., and Antiguedad, I.: Variability of particulate (SS, POC)
281 and dissolved (DOC, NO₃) matter during storm events in the Alegria agricultural watershed,
282 *Hydrological Processes*, 28, 2855-2867, 10.1002/hyp.9850, 2014.

283 Darwiche-Criado, N., Comin, F. A., Sorando, R., and Sanchez-Perez, J. M.: Seasonal variability of NO₃-
284 mobilization during flood events in a Mediterranean catchment: The influence of intensive
285 agricultural irrigation, *Agriculture Ecosystems & Environment*, 200, 208-218,
286 10.1016/j.agee.2014.11.002, 2015.

287 Eder, A., Strauss, P., Krueger, T., and Quinton, J. N.: Comparative calculation of suspended sediment
288 loads with respect to hysteresis effects (in the Petzenkirchen catchment, Austria), *Journal of*
289 *Hydrology*, 389, 168-176, 10.1016/j.jhydrol.2010.05.043, 2010.

290 Evans, C., and Davies, T. D.: Causes of concentration/discharge hysteresis and its potential as a tool
291 for analysis of episode hydrochemistry, *Water Resources Research*, 34, 129-137,
292 10.1029/97wr01881, 1998.

293 Evans, D. J., and Johnes, P.: Physico-chemical controls on phosphorus cycling in two lowland streams.
294 Part 1 - the water column, *Science of the Total Environment*, 329, 145-163,
295 10.1016/j.scitotenv.2004.02.016, 2004.

296 House, W. A., and Warwick, M. S.: Hysteresis of the solute concentration/discharge relationship in
297 rivers during storms, *Water Research*, 32, 2279-2290, 10.1016/s0043-1354(97)00473-9, 1998.

298 Jarvie, H. P., Neal, C., Williams, R. J., Neal, M., Wickham, H. D., Hill, L. K., Wade, A. J., Warwick, A.,
299 and White, J.: Phosphorus sources, speciation and dynamics in the lowland eutrophic River Kennet,
300 UK, *Science of the Total Environment*, 282, 175-203, 10.1016/s0048-9697(01)00951-2, 2002.

301 Jordan, P., Arnscheidt, A., McGrogan, H., and McCormick, S.: Characterising phosphorus transfers in
302 rural catchments using a continuous bank-side analyser, *Hydrology and Earth System Sciences*, 11,
303 372-381, 2007.

304 Klein, M.: ANTI CLOCKWISE HYSTERESIS IN SUSPENDED SEDIMENT CONCENTRATION DURING
305 INDIVIDUAL STORMS - HOLBECK CATCHMENT - YORKSHIRE, ENGLAND, *Catena*, 11, 251-257,
306 10.1016/s0341-8162(84)80024-7, 1984.

307 Langlois, J. L., Johnson, D. W., and Mehuys, G. R.: Suspended sediment dynamics associated with
308 snowmelt runoff in a small mountain stream of Lake Tahoe (Nevada), *Hydrological Processes*, 19,
309 3569-3580, 10.1002/hyp.5844, 2005.

310 Lawler, D. M., Petts, G. E., Foster, I. D. L., and Harper, S.: Turbidity dynamics during spring storm
311 events in an urban headwater river system: The Upper Tame, West Midlands, UK, *Science of the*
312 *Total Environment*, 360, 109-126, 10.1016/j.scitotenv.2005.08.032, 2006.

313 Lloyd, C. E. M., Freer, J. E., Johnes, P. J., Coxon, G., and Collins, A. L.: Discharge and nutrient
314 uncertainty: implications for nutrient flux estimation in small streams, *Hydrological Processes*, n/a-
315 n/a, 10.1002/hyp.10574, 2015.

316 Lloyd, C. E. M., Freer, J. E., Johnes, P. J., and Collins, A. L.: Using hysteresis analysis of high-resolution
317 water quality monitoring data, including uncertainty, to infer controls on nutrient and sediment
318 transfer in catchments, *Science of The Total Environment*, 543, Part A, 388-404,
319 <http://dx.doi.org/10.1016/j.scitotenv.2015.11.028>, 2016.

320 McDonald, D. M., and Lamoureux, S. F.: Hydroclimatic and channel snowpack controls over
321 suspended sediment and grain size transport in a High Arctic catchment, *Earth Surface Processes and
322 Landforms*, 34, 424-436, 10.1002/esp.1751, 2009.

323 McGonigle, D. F., Burke, S. P., Collins, A. L., Gartner, R., Haft, M. R., Harris, R. C., Haygarth, P. M.,
324 Hedges, M. C., Hiscock, K. M., and Lovett, A. A.: Developing Demonstration Test Catchments as a
325 platform for transdisciplinary land management research in England and Wales, *Environmental
326 Science: Processes & Impacts*, 10.1039/C3EM00658A, 2014.

327 Oeurng, C., Sauvage, S., and Sanchez-Perez, J.-M.: Temporal variability of nitrate transport through
328 hydrological response during flood events within a large agricultural catchment in south-west
329 France, *Science of the Total Environment*, 409, 140-149, 10.1016/j.scitotenv.2010.09.006, 2010.

330 Outram, F. N., Lloyd, C. E. M., Jonczyk, J., Benskin, C. M. H., Grant, F., Perks, M. T., Deasy, C., Burke,
331 S. P., Collins, A. L., Freer, J., Haygarth, P. M., Hiscock, K. M., Johnes, P. J., and Lovett, A. L.: High-
332 frequency monitoring of nitrogen and phosphorus response in three rural catchments to the end of
333 the 2011–2012 drought in England, *Hydrol. Earth Syst. Sci.*, 18, 3429-3448, 10.5194/hess-18-3429-
334 2014, 2014.

335 Rodriguez-Blanco, M. L., Taboada-Castro, M. M., and Taboada-Castro, M. T.: Phosphorus transport
336 into a stream draining from a mixed land use catchment in Galicia (NW Spain): Significance of runoff
337 events, *Journal of Hydrology*, 481, 12-21, 10.1016/j.jhydrol.2012.11.046, 2013.

338 Tena, A., Vericat, D., and Batalla, R. J.: Suspended sediment dynamics during flushing flows in a large
339 impounded river (the lower River Ebro), *Journal of Soils and Sediments*, 14, 2057-2069,
340 10.1007/s11368-014-0987-0, 2014.

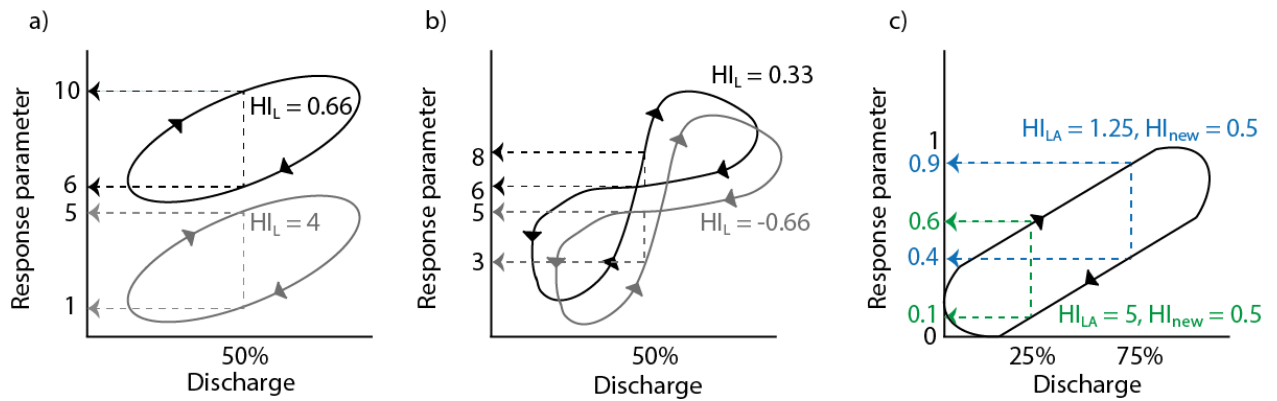
341 Whiting, P. J., Samm, J. F., Moog, D. B., and Orndorff, R. L.: Sediment-transporting flows in
342 headwater streams, *Geological Society of America Bulletin*, 111, 450-466, 10.1130/0016-
343 7606(1999)111<0450:stfihs>2.3.co;2, 1999.

344 Williams, G. P.: Sediment concentration versus water discharge during single hydrologic events in
345 rivers, *Journal of Hydrology*, 111, 89-106, 10.1016/0022-1694(89)90254-0, 1989.

346 Ziegler, A. D., Benner, S. G., Tantasirin, C., Wood, S. H., Sutherland, R. A., Sidle, R. C., Jachowski, N.,
347 Nullet, M. A., Xi, L. X., Snidvongs, A., Giambelluca, T. W., and Fox, J. M.: Turbidity-based sediment
348 monitoring in northern Thailand: Hysteresis, variability, and uncertainty, *Journal of Hydrology*, 519,
349 2020-2039, 10.1016/j.jhydrol.2014.09.010, 2014.

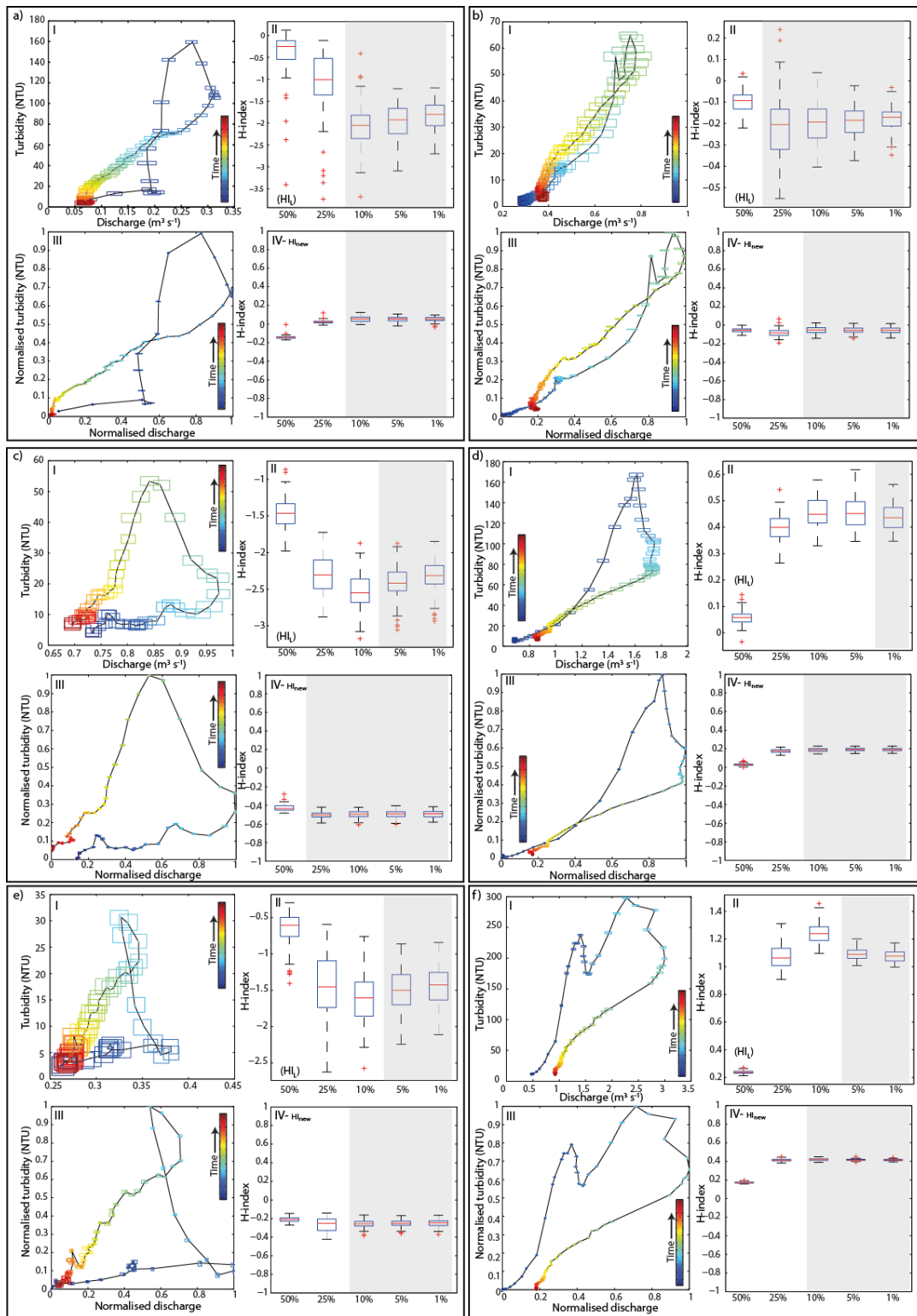
350

351



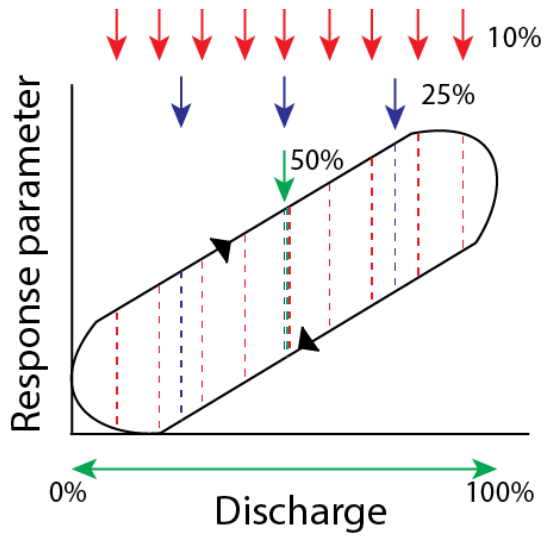
352

353 Figure 1: Plots showing a) impact of storm initial concentration, b) storm initial discharge on the
 354 value of the calculated HI when the mid-point in discharge and raw data is used and c) an idealised
 355 and normalised storm illustrating the impact of measuring different quantiles of flow on the HI
 356 calculated. Where HI_L and HI_{LA} are the original and adapted Lawler et al. (2006) methods,
 357 respectively and HI_{new} , the proposed new method. Colours represent different discharge intervals
 358 measured.



359

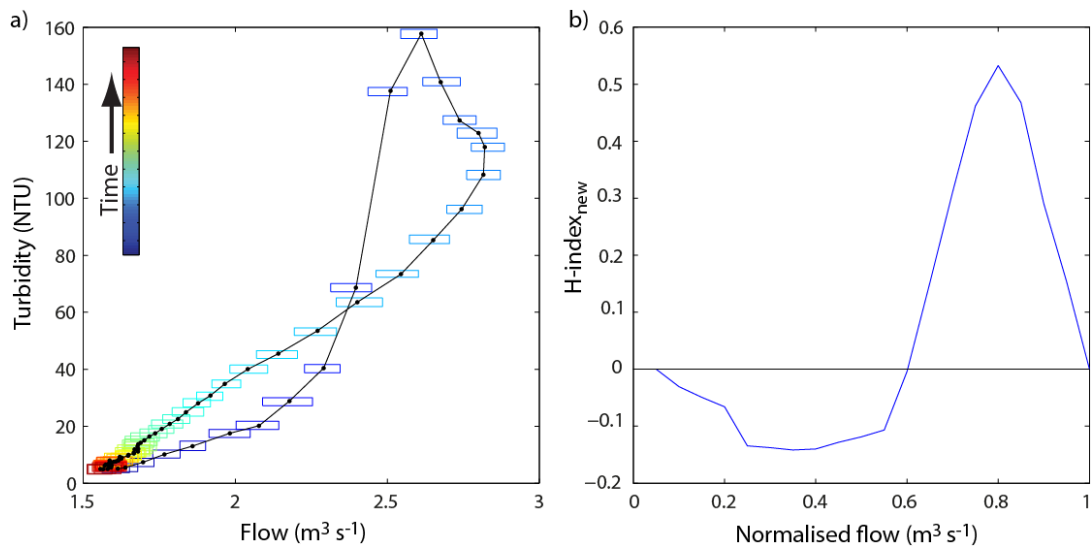
360 Figure 2: Plots showing six storms with varying loop shapes and sizes (a-f), where (I) is the hysteresis
 361 loop using the raw data, (II) is the distribution of HI values using the original and adapted Lawler et
 362 al. (2006) methods (HI_L/HI_{LA}) using varying percentiles of flow, (III) is the hysteresis loop plotted using
 363 normalised data, and (IV) is the distribution of HI values using the new method (HI_{new}) using varying
 364 percentiles of flow. The grey areas show the distributions which are not statistically different from
 365 each other. In panels I and III, the black line represents the median and the boxes represent the 5th-
 366 95th percentiles of the uncertainty range.



367

368 Figure 3: diagram showing examples of how the sampling intervals for the calculation of the HI_{LA} and
 369 HI_{new} are determined.

370



371

372 Figure 4: showing a) the original storm, where the black line represents the median and the boxes
 373 the 5th-95th percentiles of the uncertainty around the line, and b) illustrates the HI_{new} of the
 374 normalised storm.